



Measurement of the WZ and ZZ Production Cross Sections Using WZ $\rightarrow 3\ell + \cancel{E}_T$ and ZZ $\rightarrow 4\ell$ Channels

The CDF Collaboration
(Dated July 19, 2010)

Using $\sim 6 \text{ fb}^{-1}$ of data collected by the CDF experiment in $p\bar{p}$ collisions at 1.96 TeV we reconstruct 50 $WZ \rightarrow 3\ell + \nu$ candidate events, where ℓ is a charged lepton, and measure the ratio

$$\sigma(p\bar{p} \rightarrow WZ)/\sigma(p\bar{p} \rightarrow Z) = (5.5 \pm 0.9) \times 10^{-4}$$

Using 4 $ZZ \rightarrow 4\ell$ candidate events with $M(ZZ) < 300 \text{ GeV}$ we measure the ratio of the ZZ production cross section to the inclusive Z production cross section

$$\sigma(p\bar{p} \rightarrow ZZ)/\sigma(p\bar{p} \rightarrow Z) = (2.3^{+1.5}_{-0.9} \text{ (stat)} \pm 0.3 \text{ (syst)}) \times 10^{-4}$$

Taking the theoretical value of $\sigma(Z^0 \rightarrow l^+l^-)$ pb calculated in [2], we determine the diboson production cross sections

$$\sigma(p\bar{p} \rightarrow WZ) = (4.1 \pm 0.7) \text{ pb}$$

and

$$\sigma(p\bar{p} \rightarrow ZZ) = (1.7^{+1.2}_{-0.7} \text{ (stat)} \pm 0.2 \text{ (syst)}) \text{ pb}$$

Normalization to the inclusive Z production cross section reduces the systematic uncertainties on the measured cross sections.

I. INTRODUCTION

Measuring heavy diboson production in $p\bar{p}$ collisions is a way of probing the structure of the electroweak sector, and provides milestones on the way to sensitivity to rare processes such as Higgs boson production. We measure WZ and ZZ production in the three- and four-lepton channels.

This note describes the WZ and ZZ cross-section measurements. The analysis differs from previous CDF heavy diboson analyses through several reconstruction improvements that give gains in acceptance and resolution.

We recover electrons reconstructed in the region between the central and forward calorimeters by using the outermost rings of the central and forward calorimeters. We update the way in which energy leakage between calorimeter towers is taken into account in the central electron isolation computation by estimating the leakage event-by-event using spatial information from the central shower maximum detector. We improve charge reconstruction for forward electrons by running an extra pass of a tracking algorithm to associate central tracker hits with silicon-only tracks seeded by forward electron candidates.

The data used in this analysis were collected from December 2004 to May 2010, corresponding to an integrated luminosity of $\sim 6 \text{ fb}^{-1}$ and selected by the high- p_T electron and muon triggers.

II. DETECTOR DESCRIPTION

The components of the CDF II detector relevant to this analysis are described briefly here; a more complete description can be found elsewhere [1]. The detector geometry is described by the azimuthal angle ϕ and the pseudorapidity $\eta = \ln(\tan \theta/2)$, where θ is the polar angle of a particle with respect to the proton beam axis (positive z-axis). The

pseudorapidity of a particle originating from the centre of the detector is referred to as η_{det} . The trajectories of charged particles are reconstructed using silicon microstrip detectors and a 96-layer open cell drift chamber (COT) embedded in a 1.4 T solenoidal magnetic field. For $|\eta_{\text{det}}| \leq 1$ a particle traverses all 96 layers of the COT; this decreases to zero at $|\eta_{\text{det}}| \approx 2$. The silicon system provides coverage with 6 (7) layers with radii between 2.4 cm and 28 cm for $|\eta_{\text{det}}| < 1$ ($1 < |\eta_{\text{det}}| < 2$). Around the solenoid are electromagnetic (EM) and hadronic (HAD) sampling calorimeters segmented in a projective tower geometry. The first hadronic interaction length (λ) of the calorimeter, corresponding to 19-21 radiation lengths (X_0), uses lead absorber for measuring the electromagnetic component of showers, while the section extending to $4.5-7\lambda$ uses iron to contain the hadronic component. The calorimeters are divided into central $|\eta_{\text{det}}| < 1$ and forward ($1.1 < |\eta_{\text{det}}| < 3.64$) regions. Shower maximum detectors (SMX) embedded in the electromagnetic calorimeters at approximately $6 X_0$ help in the position measurement and background suppression for electrons. Around the central calorimeters are scintillators and drift chambers for identifying muons as minimum ionizing particles (CMU, CMP, CMX and BMU).

III. RECONSTRUCTION AND IDENTIFICATION

Electron candidates are required to have left only a small energy deposit in the hadronic calorimeter, to be fiducial to the shower maximum detectors and to have a shower shape consistent with that expected from an electron. The energy in a cone of $\Delta R < 0.4$ around the electron candidate is required to be less than 4 GeV after having been corrected for leakage between calorimeter wedges, using information from the shower maximum detector to localise the shower within the wedge. Candidates are required to have a well-reconstructed track that is well-matched to the reconstructed calorimeter cluster, and the energy measured in the shower maximum detector must be consistent with the measured track p_T . Central tracks are required to have χ^2 per degree of freedom < 3 . ‘Tight’ central electrons have the further requirement that the track should have ≥ 3 axial and ≥ 3 stereo track segments in the COT. Forward electron tracks must have ≥ 5 silicon hits if they are silicon-only. Electron candidates that are part of a conversion pair are rejected.

Muon candidates are required to have COT tracks with > 30 hits and $> 60\%$ of the expected number of hits. These tracks must also have χ^2 per degree of freedom < 3 . The EM and HAD energy deposits must be consistent with a minimally-ionising particle. If the track has fewer than three COT segments with 5 or more hits, extra criteria are applied to the silicon portion of the track: there must be at least 5 $r - \phi$ hits and the silicon track χ^2 must be < 100 .

Lepton candidates are required to be separated by $\Delta R > 0.005$.

Good runs are selected where for events containing only electrons, all the detector systems used to identify electrons were marked as good, and for other events all detector systems were marked as good.

IV. INCLUSIVE Z BOSON PRODUCTION IN THE $Z \rightarrow \ell\ell$ CHANNEL

We verify lepton identification and acceptance by measuring the $Z^0 \rightarrow e^+e^-$ and $Z^0 \rightarrow \mu^+\mu^-$ cross sections as a function of time for all pairs of electron and muons that are triggerable. We find the cross sections to be stable in time and consistent across channels. Examples are shown in Figure 1 for electrons and Figure 2 for muons. Combining the thirteen channels consisting of different combinations of subdetectors we measure $\sigma(pp \rightarrow Z \rightarrow \ell\ell) = 247 \pm 4$ pb.

This is to be compared with the NLO theoretical value computed by Stirling for the CDF W/Z cross section measurement of 251.3 ± 5.0 pb [2].

V. MEASUREMENT OF THE WZ PRODUCTION CROSS SECTION IN THE $WZ \rightarrow 3\ell + \cancel{E}_T$ CHANNEL

We measure the WZ production cross section in the $WZ \rightarrow 3\ell + \cancel{E}_T$ channel.

A. Event Selection

We require candidate events to contain exactly three identified leptons (electrons or muons) passing the loose identification cuts, where all leptons have $p_T > 15$ GeV, two leptons are of the same flavour, opposite charge and combine to lie in the mass window $|m_{\ell\ell} - m_Z| < 15$ GeV, and where $\cancel{E}_T > 25$ GeV.

Note that the trigger threshold is 18 GeV so that in effect at least one lepton is required to have higher p_T than the 15 GeV specified by the lepton ID cuts; this is modelled in the simulation.

B. Backgrounds

We consider backgrounds to the WZ signal coming from ZZ, $Z\gamma$ and Z+jets events.

A contribution to our selected WZ candidate events comes from ZZ events where one of the leptons escaped detection. We estimate this background using simulation normalised to the standard model cross-section of 1.6 pb [4], and find an expectation of 2.4 and 2.3 ZZ events passing our WZ selection in the $Z^0 \rightarrow e^+e^-$ and $Z^0 \rightarrow \mu^+\mu^-$ channels respectively.

Another contribution to the three-lepton event selection comes from $Z\gamma$ events. In three-lepton events with no \cancel{E}_T requirement, a component of $Z\gamma$ events with an FSR photon is clearly separated from the Z peak in the dilepton invariant mass. We therefore normalise the $Z\gamma$ contribution to our signal using the data. We use the Baur $Z\gamma$ simulation, and normalise it to the data in the region $40 < m_{\ell\ell} < 80$ GeV as shown in Fig 3. We then use the Baur simulation to find the contribution to the WZ selection at high \cancel{E}_T . We find an expectation of 1.6 and 0.7 events in the $Z^0 \rightarrow e^+e^-$ and $Z^0 \rightarrow \mu^+\mu^-$ channels respectively.

A further contribution to our event selection comes from events containing an object reconstructed incorrectly as a lepton. The main source of this background is Z+jets events where the jet fakes an electron or muon. Our strategy is to measure fake rates with respect to clusters reconstructed in the electromagnetic calorimeter for electrons, and with respect to high-quality isolated tracks for muons, and to apply them to the inclusive Z Monte Carlo. Fake rates are of the order of 5% and we estimate backgrounds of 2.4 and 1.8 events in the $Z^0 \rightarrow e^+e^-$ and $Z^0 \rightarrow \mu^+\mu^-$ channels respectively.

The backgrounds are summarized in Table I.

	WZ($Z \rightarrow ee$)	WZ($Z \rightarrow \mu\mu$)
ZZ	2.4 ± 0.2	2.3 ± 0.2
$Z\gamma$	1.6 ± 0.6	0.7 ± 0.3
Z+jets	2.4 ± 1	1.8 ± 1
Total	6.4 ± 1.2	4.8 ± 1.1

TABLE I: Summary of WZ backgrounds

C. Systematic Uncertainties

We consider sources of systematic uncertainty contributing more than 0.5%.

Lepton identification and reconstruction efficiencies are estimated to contribute a 6% uncertainty to the measured cross section. This is expected to be reduced in future.

Systematic uncertainties on the acceptance arise from several sources. Uncertainties in the knowledge of the detector geometry are either absorbed by the ID scale factors or partially cancel from the ratio $\sigma(VV)/\sigma(Z^0 \rightarrow l^+l^-)$.

To calculate the acceptance we use Pythia, which is a leading order ME event generator. We estimate the effect of NLO corrections on the acceptance uncertainties by comparing Pythia to MC@NLO+Herwig.

MC@NLO is a NLO matrix element event generator interfaced to HERWIG, which models fragmentation of the partons produced in the hard interaction. When comparing output of Pythia and MC@NLO it is therefore important to distinguish between the NLO effects and differences between the Pythia and HERWIG fragmentation models.

As MC@NLO generates a diboson pair with average $PT=0$, by comparing MC@NLO to Pythia it is only possible to study NLO effects on the $M(WZ)$ and rapidity distributions of the vector bosons. $M(WZ)$ is correlated with the transverse momentum of the vector bosons and also with differences in their rapidities. We compare $M(WZ)$ distributions generated by Pythia and MC@NLO and assume that differences between these distributions effectively absorb most of the NLO effects. We use it to weight events generated by Pythia to estimate the effect of NLO corrections on the acceptance. We find that NLO effects increase the WZ acceptance, however the net effect is small and we estimate it to be 1.1%.

Parton momenta distributions are known to finite accuracy and their variations affect the calculated acceptance. To estimate the effect of PDF uncertainties on the acceptance we parameterise the lepton efficiencies in η and apply them to generator-level events. We weight each event according to the 40 CTEQ6 error sets and combine the results according to the CTEQ prescription. We find the total uncertainty on the WZ acceptance is less than 0.5%.

As we normalize results of the measurement to the $Z^0 \rightarrow l^+l^-$ cross section, the systematic uncertainty on the luminosity cancels out from the ratio, replaced by the uncertainty on the cross section ratio $\sigma(WZ)/\sigma(Z^0 \rightarrow l^+l^-)$

resulting from the uncertainties in PDFs. To evaluate this uncertainty we use the CTEQ6 ‘PDF error sets’ again. We find that the correlation between $\sigma(WZ)$ and $\sigma(Z^0 \rightarrow l^+l^-)$ is positive so PDF uncertainties on the total cross sections partially cancel out in the ratio $\sigma(WZ)/\sigma(Z^0 \rightarrow l^+l^-)$. The remaining uncertainty is found to be asymmetric $\sigma_{PDF} = {}^{+2.7\%}_{-1.8\%}$; without knowing which exactly physics effect is causing the asymmetry, we quote a symmetric error $\sigma_{PDF}(\sigma(WZ)/\sigma(Z^0 \rightarrow l^+l^-)) = \pm 2.7\%$.

D. Cross section

Table II contains a summary of the inputs used for the cross section calculation. Integrated luminosities corresponding to electron-only and electron+muon good run lists differ by 3.5%; we use acceptance-weighted averages.

Dividing the measured acceptance by the branching ratios $\text{BR}(W \rightarrow (e \text{ or } \mu) \times Z^0 \rightarrow e^+e^-)$ gives an impression of the fraction of events in each final state that we measure, and is around 14% per Z final state (the acceptance computation from the Monte Carlo also includes the contribution from $W \rightarrow \tau$, which is suppressed by the τ leptonic branching ratio and the lepton p_T requirements).

Accounting for the trigger, reconstruction and ID efficiency scale factors introduces a correction of 0.84 for $WZ(Z \rightarrow ee)$ and of 0.77 for $WZ(Z \rightarrow \mu\mu)$. This includes the zeroing of non-triggerable events.

Input	WZ(Z \rightarrow ee)	WZ(Z \rightarrow $\mu\mu$)
N(signal)	28	22
Background	6.4 ± 1.2	4.8 ± 1.1
Acceptance	$(0.997 \pm 0.036 \text{ (MC stat)}) \times 10^{-3}$	$(0.981 \pm 0.036 \text{ (MC stat)}) \times 10^{-3}$
Scale Factors(ID+trig+reco)	0.84 ± 0.05	0.77 ± 0.05
L_{int}/fb	6.04 ± 0.36	5.86 ± 0.35

TABLE II: Inputs for the $p\bar{p} \rightarrow WZ$ cross section calculation

The calculated cross section is

$$\sigma(p\bar{p} \rightarrow WZ(Z \rightarrow ee)) = (4.3 \pm 0.8(stat) \pm 0.5(syst))\text{pb}$$

$$\sigma(p\bar{p} \rightarrow WZ(Z \rightarrow \mu\mu)) = (3.9 \pm 0.8(stat) \pm 0.4(syst))\text{pb}$$

Normalizing the measured value of $\sigma(p\bar{p} \rightarrow WZ)$ to the measured value of $\sigma(p\bar{p} \rightarrow Z) \cdot \text{B}(Z \rightarrow ll)$ we obtain

$$\frac{\sigma(p\bar{p} \rightarrow WZ)}{\sigma(p\bar{p} \rightarrow Z)} = (5.5 \pm 0.8(stat) \pm 0.5(syst))10^{-4}$$

Using a NNLO calculation of the $\sigma(p\bar{p} \rightarrow Z) \cdot \text{B}(Z \rightarrow ll) = 251.3 \pm 5$ [2] gives the cross section

$$\sigma(p\bar{p} \rightarrow WZ) = (4.1 \pm 0.6(stat) \pm 0.4(syst))\text{pb}$$

which has several experimental systematic uncertainties, including uncertainty on the integrated luminosity, cancelled out. We expect the systematic uncertainty on the scale factor correction to be reduced in future. Figures 4 to 11 show properties of the candidate events.

VI. MEASUREMENT OF THE ZZ PRODUCTION CROSS SECTION IN THE $ZZ \rightarrow 4l$ CHANNEL

We use the all-leptonic final state $ZZ \rightarrow 4l$ to measure the ZZ production cross section in $p\bar{p}$ collisions. This measurement is complementary to a search for high-mass ZZ resonances, an analysis currently in progress.

In order not to unblind the data in the high-mass region, $M(ZZ) > 300$ GeV, we use a low mass region, $M(ZZ) < 300$ GeV, to measure the ZZ production cross section.

A. Event Selection

Selection of the ZZ candidate events starts from selecting events with exactly 4 identified leptons: one with $p_T > 20$ GeV and the others above 15 GeV, and the invariant mass of the 4 leptons less than $300 \text{ GeV}/c^2$.

No charge or flavour matching is required at this step.

There are 6 candidate events with 4 identified leptons.

In all of these events the total charge of the 4 leptons is zero and all events have an even number (0, 2 or 4) of leptons of the same flavour.

Leptons of the same flavour are combined into pairs to create 2 Z candidates in the event. In case the association is ambiguous ($4e$ or 4μ), the best combination is required to minimize the χ^2 of the ZZ hypothesis

$$\chi^2 = (M_{12} - M_Z)^2/\sigma(M_{12})^2 + (M_{34} - M_Z)^2/\sigma(M_{34})^2$$

To minimize effects of Z/γ^* interference, both Z candidates are required to have invariant masses within 15 GeV from the Z boson mass, i.e. in the range of 76-106 GeV. This requirement leaves 4 candidate events.

Although not required by the selection procedure, all Z candidates in all 4 events have zero reconstructed charge.

We note that a looser requirement for both Z candidates in an event to have their invariant masses above 60 GeV leaves the same 4 events.

B. Backgrounds

The $ZZ \rightarrow 4l$ final state is the only SM process resulting in the final state with 4 high- p_T leptons produced in the primary interaction, so the background in this channel comes only from the mis-identification.

The following SM processes contribute the most.

- $p\bar{p} \rightarrow WZ + jet$ with a jet misidentified as a lepton
- $p\bar{p} \rightarrow Z + 2jets$ with both jets misidentified as a lepton
- $p\bar{p} \rightarrow Z\gamma + jet$ with the converted photon misidentified as an electron and the jet faking an electron

The contribution of $t\bar{t}$ production is an order of magnitude less than that from production.

We rely on Monte Carlo to simulate kinematics of the processes above and use the jet-to-lepton misidentification rates measured in the inclusive jet data to weight the MC events and estimate the expected yield of the background events. The total background from the processes above is estimated to be less than 0.01 events.

C. Systematic Uncertainties

Systematic uncertainties are assessed in the same way as in the WZ cross-section measurement and are summarized in Table III.

Source	Value
ID efficiency	6%
Trigger Efficiency	2%
PDFs	2.7%
NLO effects	2.7%

TABLE III: Summary of systematic uncertainties in the $ZZ \rightarrow 4l$ channel

D. Cross section

Table IV contains summary of the inputs used for the cross section calculation.

The statistical uncertainty on the measured cross section is estimated using the method proposed by Feldman and Cousins [3], with a 68% confidence level interval.

Input	Value
N_{SIGNAL}	4
N_{BGR}	<0.01
Acceptance ($M(\text{ZZ}) < 300$)	0.11
$BR(Z^0 \rightarrow l^+l^-)^2$	4.52×10^{-3}
Scale Factors(ID+trig+reco)	0.8 ± 0.08
$L_{\text{int}}, \text{fb}^{-1}$	5.91 ± 0.35

TABLE IV: Inputs for the $p\bar{p} \rightarrow ZZ$ cross section calculation

The calculated cross section is

$$\sigma(p\bar{p} \rightarrow ZZ) = (1.7_{-0.7}^{+1.2}(\text{stat}) \pm 0.2(\text{syst}) \pm 0.1(\text{lumi}))\text{pb}$$

Normalizing the measured value of $\sigma(p\bar{p} \rightarrow ZZ)$ to the measured value of $\sigma(p\bar{p} \rightarrow Z) * B(Z \rightarrow ll)$ we obtain

$$\frac{\sigma(p\bar{p} \rightarrow ZZ)}{\sigma(p\bar{p} \rightarrow Z)} = (2.3_{-0.9}^{+1.5}(\text{stat}) \pm 0.27(\text{syst}))10^{-4}$$

Using a NNLO calculation of the $\sigma(p\bar{p} \rightarrow Z) \times B(Z \rightarrow ll) = 251.3 \pm 5$ [2] gives the cross section

$$\sigma(p\bar{p} \rightarrow ZZ) = (1.7_{-0.7}^{+1.2}(\text{stat}) \pm 0.2(\text{syst}))\text{pb}$$

which has several experimental systematic uncertainties, including uncertainty on the integrated luminosity, cancelled out.

VII. CONCLUSIONS

We have measured the WZ production cross section at 1.96 TeV to be

$$\sigma(p\bar{p} \rightarrow WZ) = (4.1 \pm 0.6(\text{stat}) \pm 0.4(\text{syst}))\text{pb}$$

and the ZZ production cross section to be

$$\sigma(p\bar{p} \rightarrow ZZ) = (1.7_{-0.7}^{+1.2}(\text{stat}) \pm 0.2(\text{syst}))\text{pb}.$$

Acknowledgments

We thank the Fermilab staff and the technical staffs of the participating institutions for their vital contributions. This work was supported by the U.S. Department of Energy and National Science Foundation; the Italian Istituto Nazionale di Fisica Nucleare; the Ministry of Education, Culture, Sports, Science and Technology of Japan; the Natural Sciences and Engineering Research Council of Canada; the National Science Council of the Republic of China; the Swiss National Science Foundation; the A.P. Sloan Foundation; the Bundesministerium für Bildung und Forschung, Germany; the World Class University Program, the National Research Foundation of Korea; the Science and Technology Facilities Council and the Royal Society, UK; the Institut National de Physique Nucleaire et Physique des Particules/CNRS; the Russian Foundation for Basic Research; the Ministerio de Ciencia e Innovación, and Programa Consolider-Ingenio 2010, Spain; the Slovak R&D Agency; and the Academy of Finland.

[1] R. Blair et al., The CDF Collaboration, FERMILAB-PUB-96/390-E (1996).

[2] The CDF Collaboration, Measurements of Inclusive W and Z Cross Sections in $p\bar{p}$ Collisions at $\sqrt{s} = 1.96$ TeV. J Phys G **34** 2457 (2007), hep-ex/0508029.

[3] G. Feldman and R. Cousins, Unified approach to the classical statistical analysis of small signals. Phys. Rev. D **57** 3873 (1998).

[4] J.M.Campbell and R.K.Ellis, Update on vector boson production at hadron colliders. Phys. Rev. D **60** 113006 (1998).

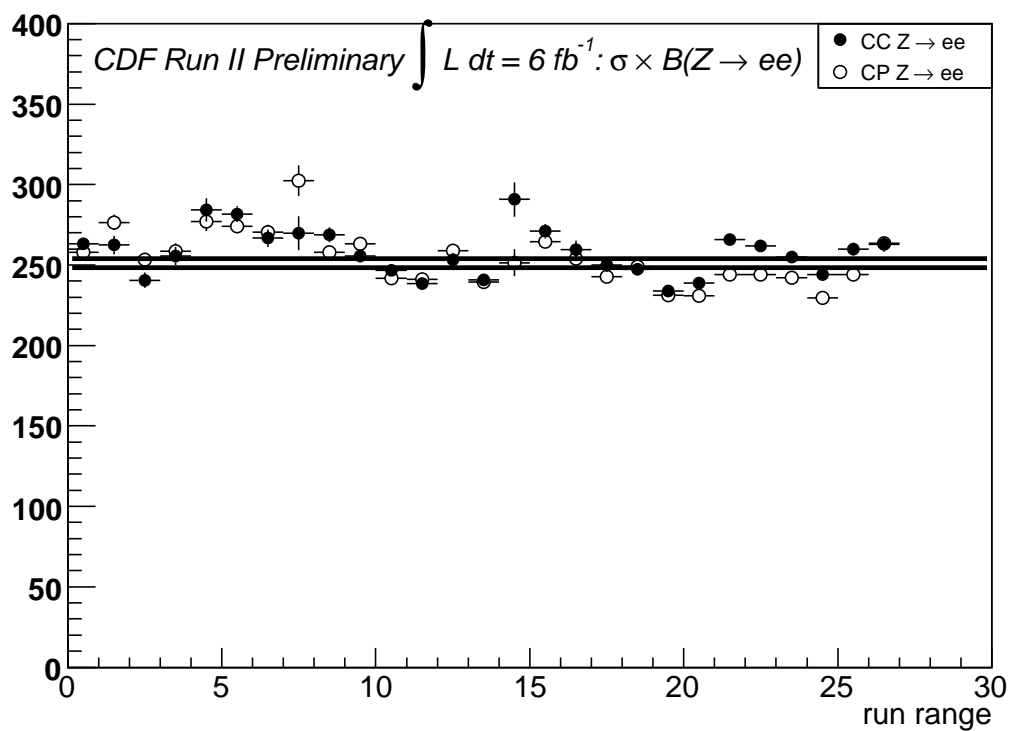


FIG. 1: $\sigma(p\bar{p} \rightarrow Z \rightarrow ee)$ for central-central and central-forward events.

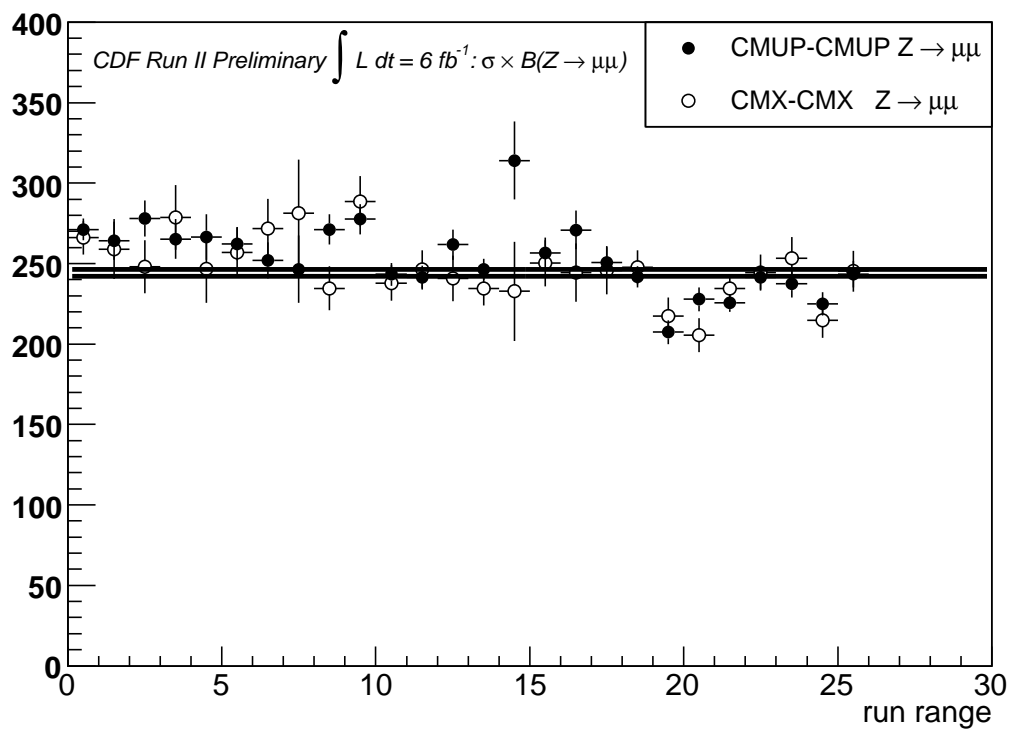


FIG. 2: Example $\sigma(p\bar{p} \rightarrow Z \rightarrow \mu\mu)$, shown here for CMUP-CMUP and CMX-CMX events.

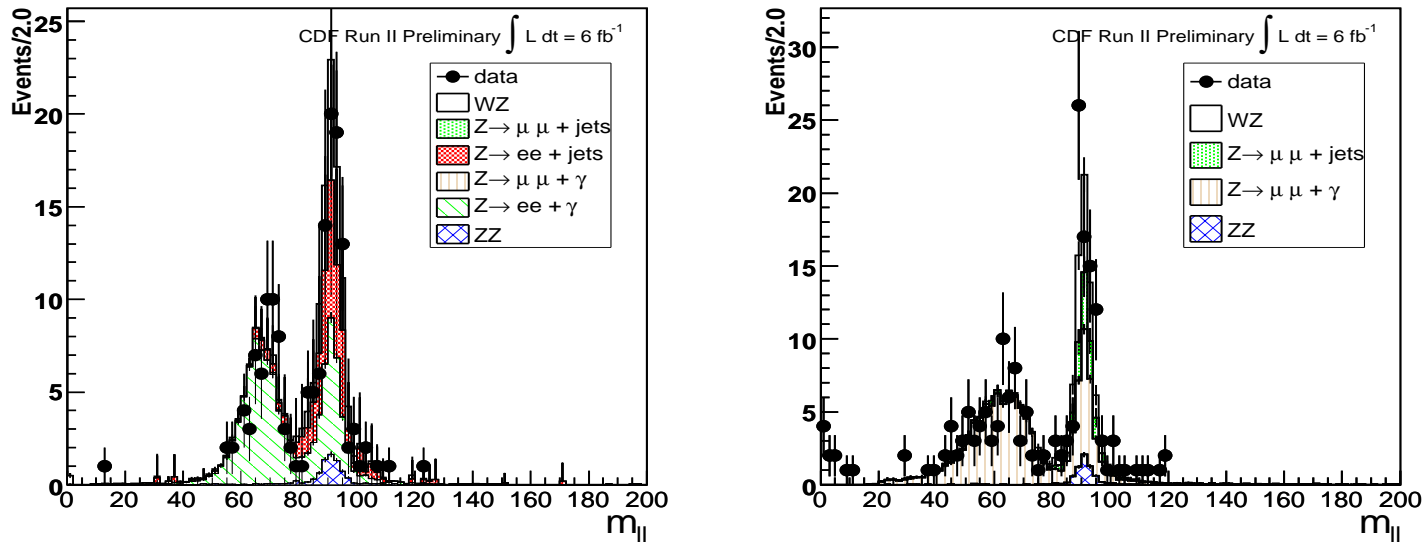


FIG. 3: Z candidate invariant mass before applying the E_T cut, after fitting for $Z\gamma$. Left: $Z^0 \rightarrow e^+e^-$; right: $Z^0 \rightarrow \mu^+\mu^-$.

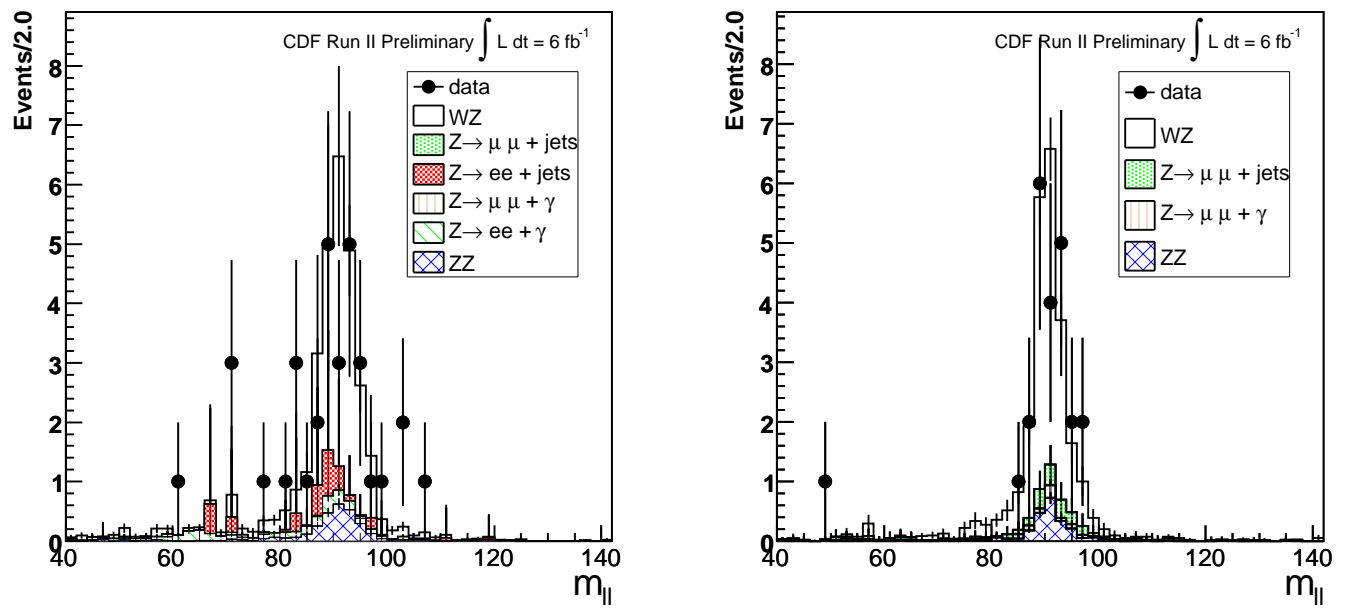


FIG. 4: Z candidate invariant mass in WZ events, before applying the tight Z mass window. Left: $Z^0 \rightarrow e^+e^-$; right: $Z^0 \rightarrow \mu^+\mu^-$.

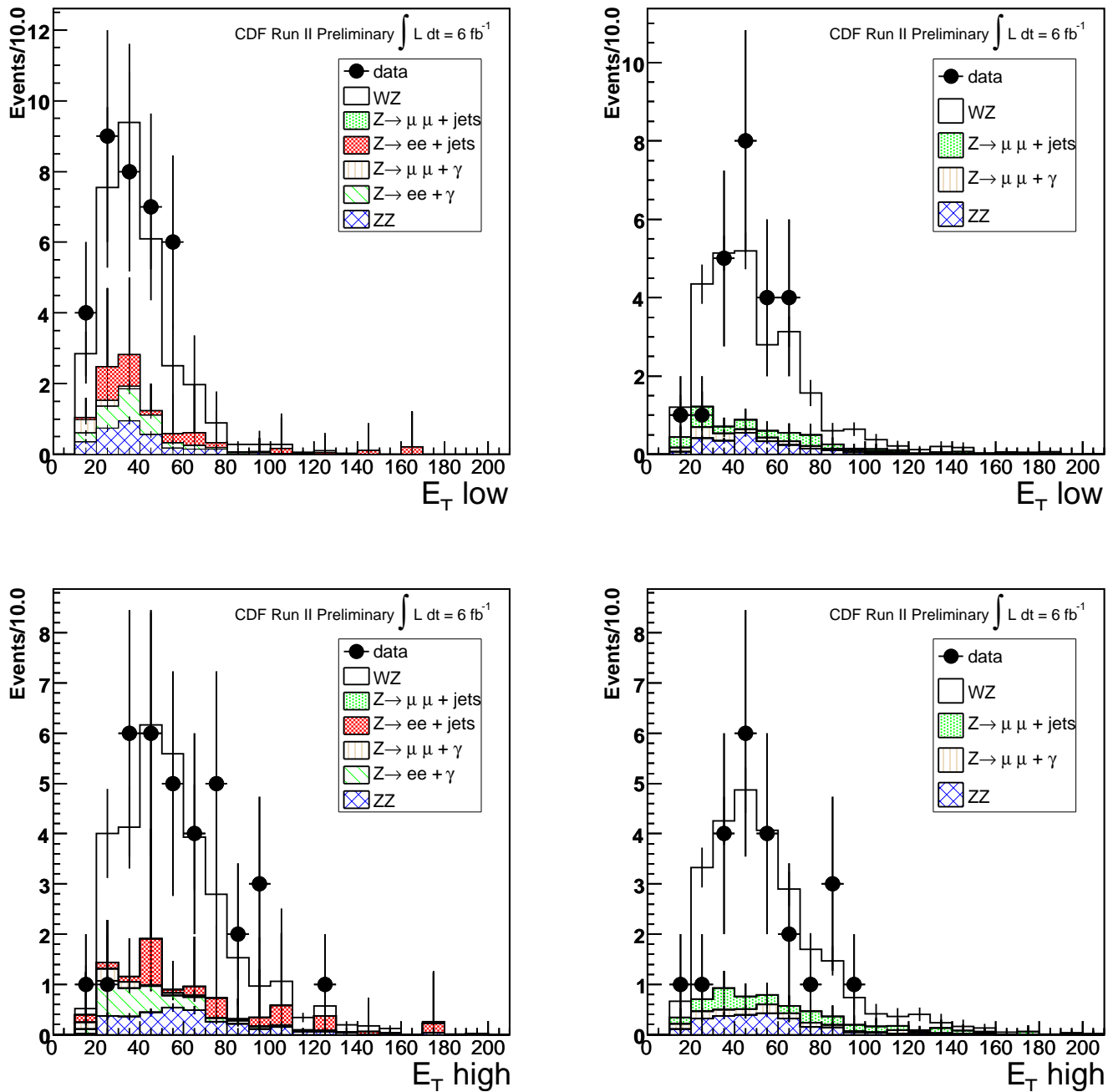


FIG. 5: Z candidate lepton p_T in WZ events before applying the tight Z mass window. Left: $Z^0 \rightarrow e^+e^-$; right: $Z^0 \rightarrow \mu^+\mu^-$. Top: low p_T leg; right: high p_T leg.

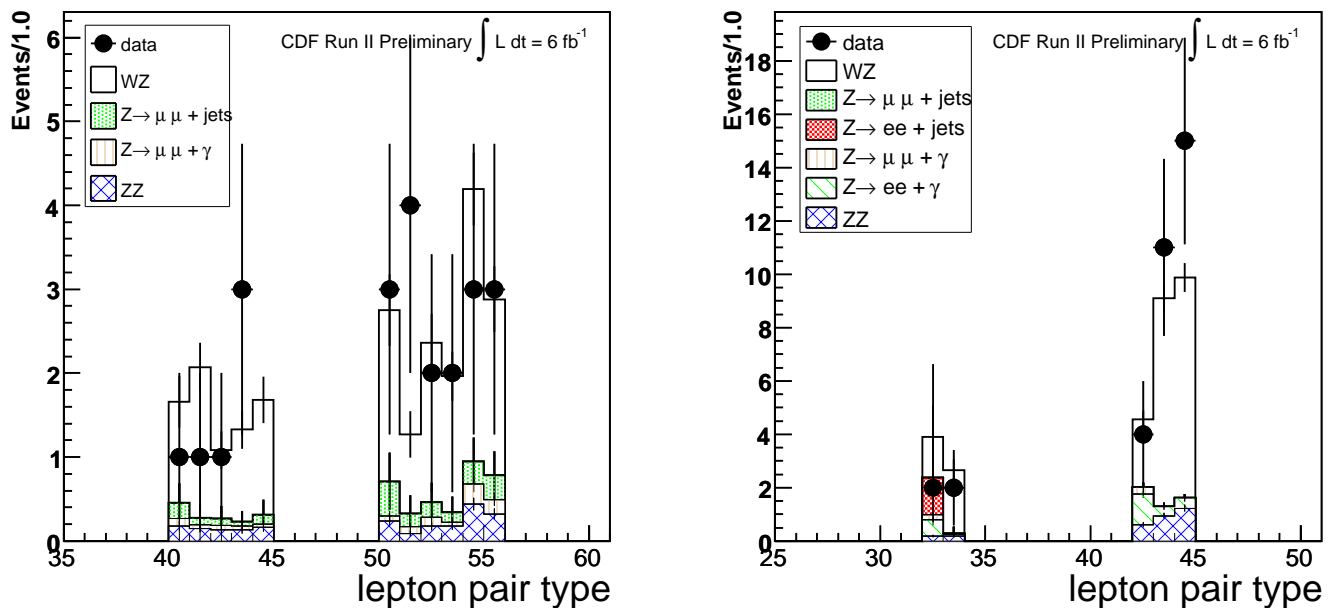


FIG. 6: Z candidate dilepton code in WZ events before applying the tight Z mass window. Left: $Z^0 \rightarrow e^+e^-$; right: $Z^0 \rightarrow \mu^+\mu^-$.

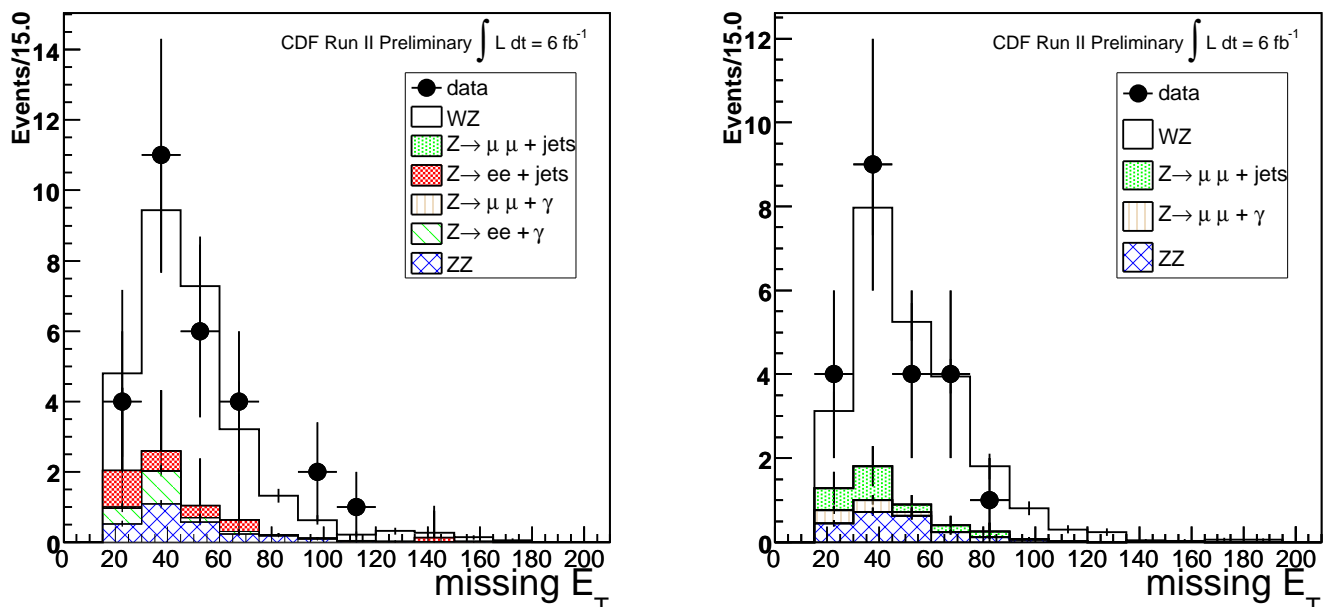


FIG. 7: Missing E_T for WZ candidates. Left: $Z^0 \rightarrow e^+e^-$; right: $Z^0 \rightarrow \mu^+\mu^-$.

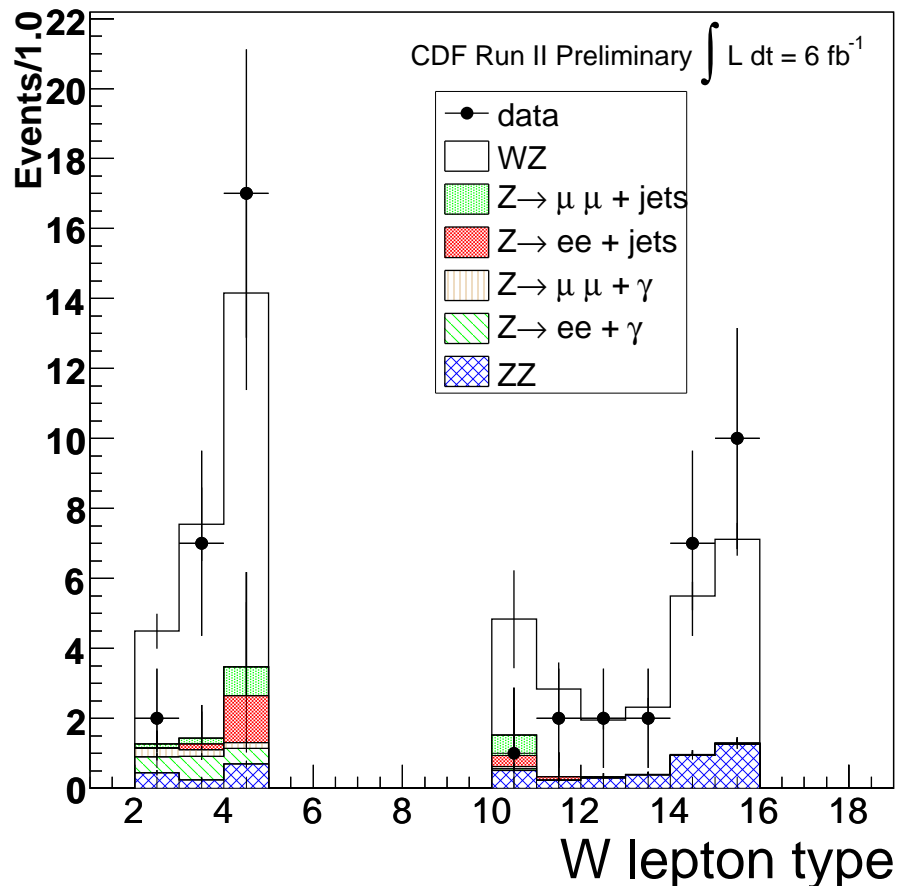


FIG. 8: Lepton type for the third lepton in WZ candidates.

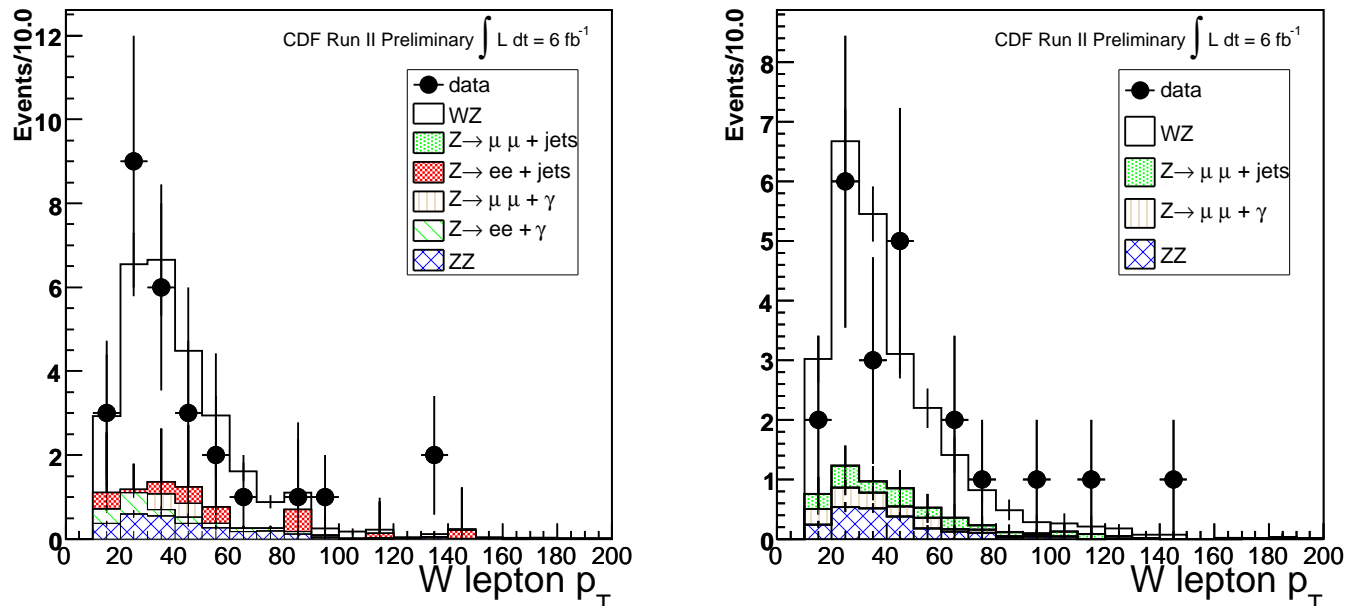


FIG. 9: p_T of the third lepton for WZ candidates. Left: $Z^0 \rightarrow e^+e^-$; right: $Z^0 \rightarrow \mu^+\mu^-$.

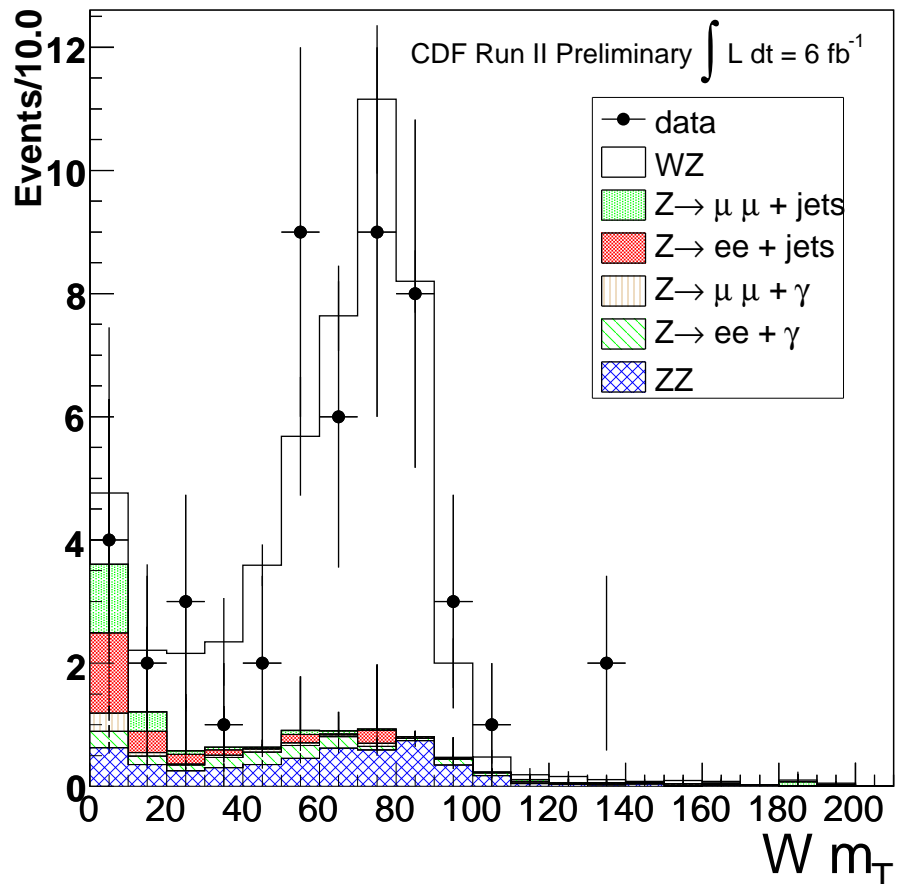


FIG. 10: Transverse mass of the W in WZ candidates.

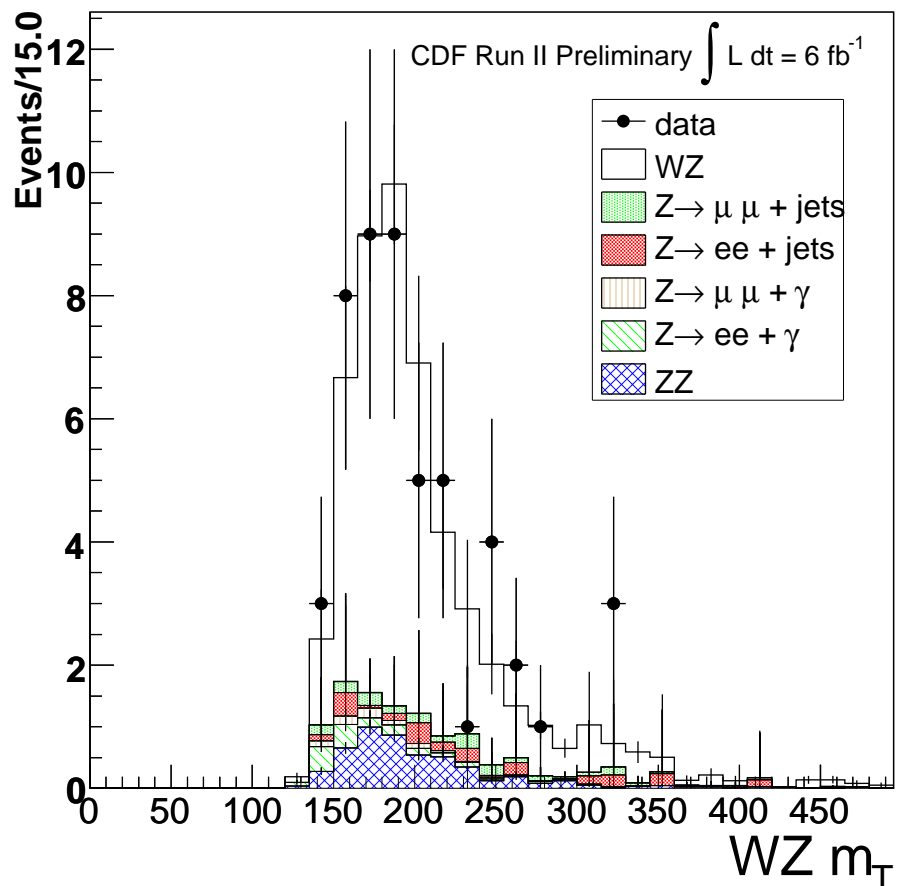


FIG. 11: Transverse mass of the WZ system.

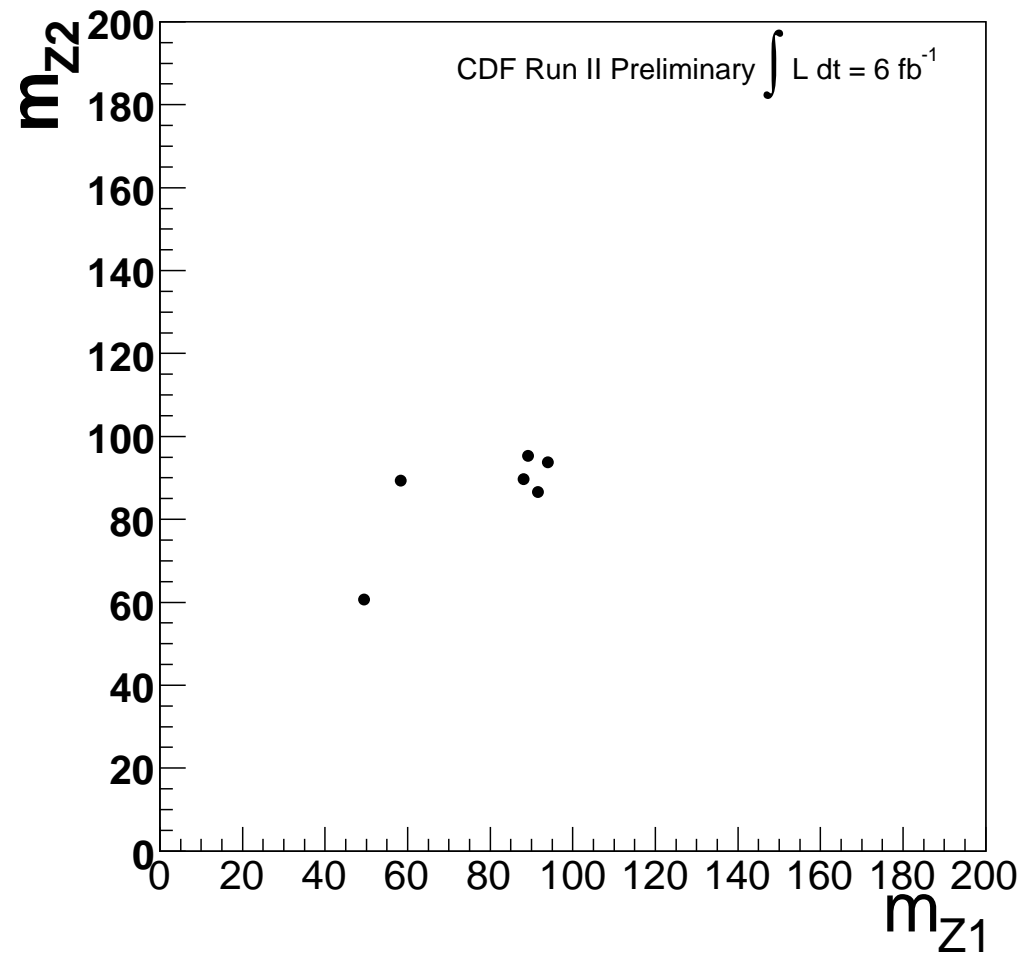


FIG. 12: The invariant mass of the two Z candidates in the 4-lepton events. Four events survive the final tight Z mass requirement.

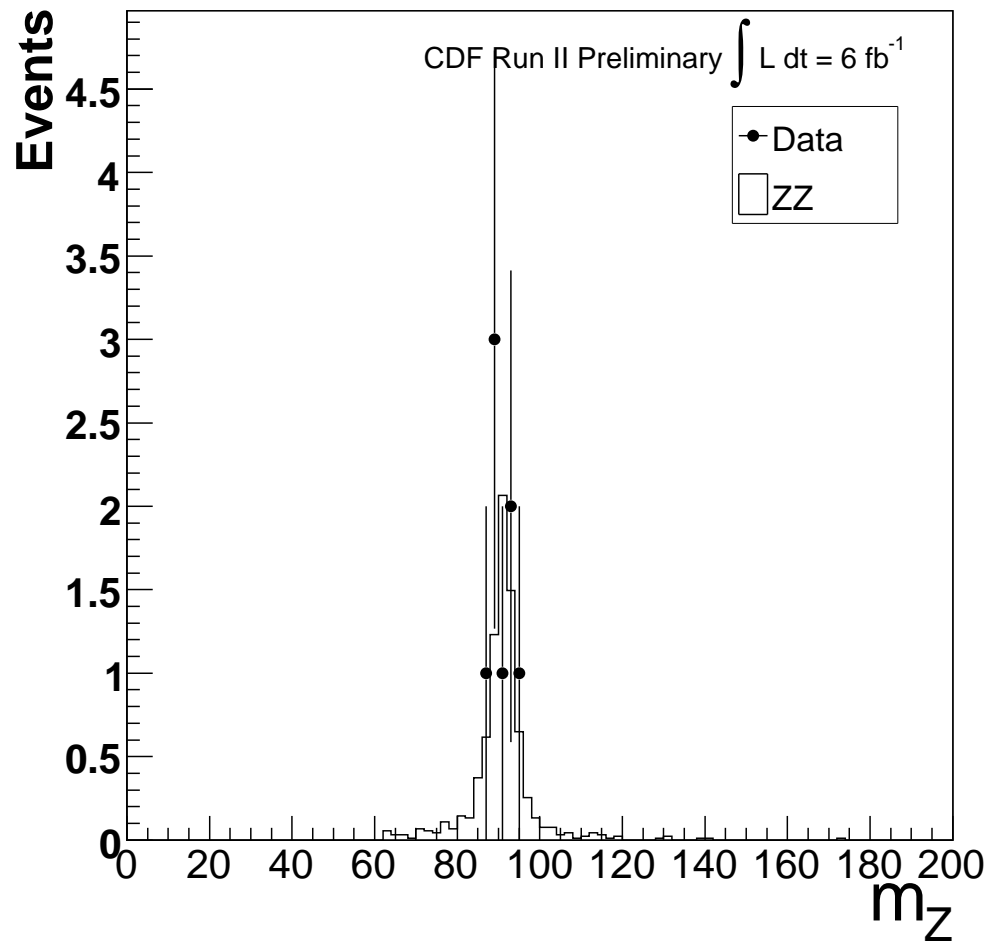


FIG. 13: Distribution in $M(\ell\ell)$ for the Z candidates reconstructed in 4 ZZ candidate events